Hindawi Publishing Corporation
International Journal of Geophysics
Volume 2014, Article ID 514937, 9 pages
http://dx.doi.org/10.1155/2014/514937

Research Article

Airglow Measurements of Gravity Wave Propagation and Damping over Kolhapur (16.5°N, 74.2°E)

R. N. Ghodpage,[1] A. Taori,[2] P. T. Patil,[1] S. Gurubaran,[3] A. K. Sharma,[4] S. Nikte,[4] and D. Nade[4,5]

[1] *MF Radar, Indian Institute of Geomagnetism, Kolhapur 416004, India*
[2] *National Atmospheric Research Laboratory, Gadanki 517112, India*
[3] *Indian Institute of Geomagnetism, Navi Mumbai 410218, India*
[4] *Department of Physics, Shivaji University, Kolhapur 416004, India*
[5] *Department of Physics, Sanjay Ghodawat Group of Institutions, Atigre, Kolhapur 41611, India*

Correspondence should be addressed to A. Taori; alok.taori@gmail.com

Received 1 May 2014; Revised 12 June 2014; Accepted 12 June 2014; Published 7 July 2014

Academic Editor: Steve Milan

Simultaneous mesospheric OH and O (^{1}S) night airglow intensity measurements from Kolhapur (16.8°N, 74.2°E) reveal unambiguous gravity wave signatures with periods varying from 01 hr to 9 hr with upward propagation. The amplitudes growth of these waves is found to vary from 0.4 to 2.2 while propagating from the OH layer (~87 km) to the O (^{1}S) layer (~97 km). We find that vertical wavelength of the observed waves increases with the wave period. The damping factors calculated for the observed waves show large variations and that most of these waves were damped while traveling from the OH emission layer to the O (^{1}S) emission layer. The damping factors for the waves show a positive correlation at vertical wavelengths shorter than 40 km, while a negative correlation at higher vertical wavelengths. We note that the damping factors have stronger positive correlation with meridional wind shears compared to the zonal wind shears.

1. Introduction

Upward propagation of gravity waves and tides is an important aspect in studying dynamical coupling between different regions in earth's atmosphere (e.g., [1]). Though the negative density gradient and conservation of energy suggest that the amplitudes of these waves grow exponentially with altitudes, dissipation processes (such as saturation and interaction of these waves with background wind and other waves) limit the amplitude growth of these waves (e.g., [2]). Information on these gravity waves and tides in upper mesosphere is considered important because of their potential association with ionospheric phenomena [3–9]. Passive airglow monitoring is a simple and cost effective method which provides required temporal resolution to study the short period gravity waves with periodicity. In particular, OH (peak emission altitude ~87 km), O_2 (peak emission altitude ~94 km), and O (^{1}S) (peak emission altitude ~97 km) emissions are often utilized to measure and characterize the upper mesospheric gravity waves (e.g., [10–12]). Upward propagating gravity waves with vertical wavelengths larger than the airglow layer thickness (typical full width at half maxima, 10 km) can be observed at multiple airglow emissions almost simultaneously. Such data can be used to estimate the amplitude growth and the propagation characteristics of gravity waves [13–15]. Taori et al. [16] utilized more than two years of OH and O_2 temperature data from Maui (20.8°N, 156.2°W) to study the amplitude growth for long as well as short period waves and found strong dissipation during summer time. Recently, Liu and Swenson [17] and Vargas et al. [18] provided a numerical model to study gravity wave induced oscillations in the airglow emission intensity and temperatures where they suggested the wave amplitudes have the following relation:

$$A_z = A_0 e^{(1-\beta)z/2H}. \quad (1)$$

In the above equation, A_0 is wave amplitude at OH emission, A_z is the amplitude at O (^{1}S) emission, z is the height difference between OH and O (^{1}S) emission layers, β is the damping factor, and H is scale height.

The quantity "β" indicates whether the observed waves were freely propagated, saturated, or damped. In a case when $\beta = 0$, (1) yields $A_z = A_0 e^{z/2H}$, which suggests exponential growth of wave amplitudes, that is, free propagation of waves in an ideal atmosphere without any dissipation. Similarly, $\beta < 1$ suggests waves grow lesser than the case when $\beta = 0$, while $\beta > 1$ suggests strong damping. In references [18, 19] investigated the airglow data obtained over Rikubetsu (43.5°N, 143.8°E) and reported the damping factor for the waves observed during March 2004 to August 2005. They found that most of the waves observed at OH and O_2 emissions simultaneously were dominated by the damping.

As far as the Indian sector is concerned, reports of multiple airglow emission monitoring at mesospheric altitudes to study vertical propagation are limited [8, 20, 21]. In the present investigation, we use the mesospheric OH (peak emission altitude ~87 km) and O (^{1}S) (peak emission altitude ~97 km) airglow emission intensity data obtained during February-March 2010 from Kolhapur (16.8°N, 74.2°E) to study propagation characteristics and amplitudes of gravity waves. We report new data on damping factors of various dominant waves and their possible association with mesospheric winds.

2. Instrumentation and Data Description

We use collocated airglow and wind measurements from Kolhapur, the description of which is as follows.

2.1. Mesospheric Airglow Data. The mesospheric OH and O (^{1}S) emission monitoring is done with the help of a photomultiplier tube (EMI-9658B) based photometer having a full field of view of 10°. The temperature stabilized interference filters are mounted on a computer controlled filter-wheel with integration time at each filter ~10 s. The interference filters mounted on filter-wheel have full width and half maxima of ~0.8 nm and are maintained at 25°C. Details of the instrument and method of temperature retrieval are discussed elsewhere [22]. The errors arising due to the photomultiplier electronics (dark current and readout noise) and filter movement are about 0.2% at 25°C. The present data are obtained for zenith viewing during February and March 2010 when clear, moonless night conditions allowed more than 6 hours of observations consecutively for 14 nights. Though photometer is capable of measuring the temperatures, in the present study, we utilize only intensity data collected at OH and O (^{1}S) emissions because the wave induced perturbations were larger in intensity data (e.g., [23]). Note that the quantities measured with any airglow photometer are the integrated emission rates, which are termed as "intensity." In the present case we measure intensity in relative units as the photometer has not been calibrated.

2.2. Mesospheric Wind Data. The mesospheric winds were obtained from the medium frequency (MF) radar operating at 2 MHz. The radar makes use of spaced antenna technique and samples the horizontal winds in the 78 to 98 km altitude region using the full correlation analysis [24]. For a suitable comparison with the night time airglow data, in the present study, we utilize the averaged wind profiles obtained during 1800–2800 (i.e., 0400) h IST to understand the mean nighttime mesospheric wind variability and their suitable association with observed nocturnal mesospheric wave characteristics.

3. Results and Discussion

3.1. Observed Wave Characteristics. It is important to state here that airglow emission altitudes show long term variability (e.g., [25]). However, as the emission altitude variation is <2 km over low and equatorial latitudes, in this paper, we have assumed that peak emission altitude does not vary significantly within a night. The intensity variability in a given night results from the superposition of various wave components prevailing on that night, which encompasses long-period planetary waves, tidal waves, and highly varying short period gravity wave. As the nightly data utilized in this study are confined to <12 hour duration, waves with periodicity longer than 12 hr may create only a slow moving trend in the data. In this regard, to identify the dominant short period waves, we remove the nightly average values (arithmetic mean of nocturnal data on a given night) from the data and obtain the deviations from the nightly average. Further, for a suitable comparison of gravity waves and their amplitudes on all the nights, we normalize the mean deviations to their nightly average values to get the percentage intensity variation. We use these percentage intensity variations to assess the wave characteristics. Note that there may be a contribution from tidal oscillations in the data which may cause error in the estimation of wave characteristics. However, we believe that simple best-fit cosine model is suitable to obtain the most probable solution (e.g., [15]). In doing so, we restrict the investigations to only two most dominant wave measurements on a given night.

Figure 1 exhibits nocturnal data obtained on the night of February 9, 2010 to illustrate (a) the complicated nocturnal variability in the presence of multiple waves in the data and (b) our best-fit method of approximation for dominant wave identification in the nocturnal data. Figures 1(a) and 1(c) show the normalized mean deviations (in percentage variability) in OH (Figure 1(a)) and O (^{1}S) emission intensity data. The solid red lines in each plot show results of the best-fit cosine model. We note that the mean intensity deviation data in OH emission are dominated by the 8.4 ± 0.5 hr wave with amplitude ~4% (Figure 1(a)). It is noteworthy that the time length of nighttime airglow monitoring is limited to 9 hours and as per the Nyquist criteria, it is difficult to estimate the periods of the same or larger oscillation. To avoid the problems associated with this, we perform the best-fit analysis for a wide range of waves with periods varying from 6 hr to 12 hr and select the wave parameters for which the χ^2 values are close to 1, suggesting the best possible explanation of the variability. As an example, the wave-fitting corresponding to periods 7 hr and 9 hr is also shown in

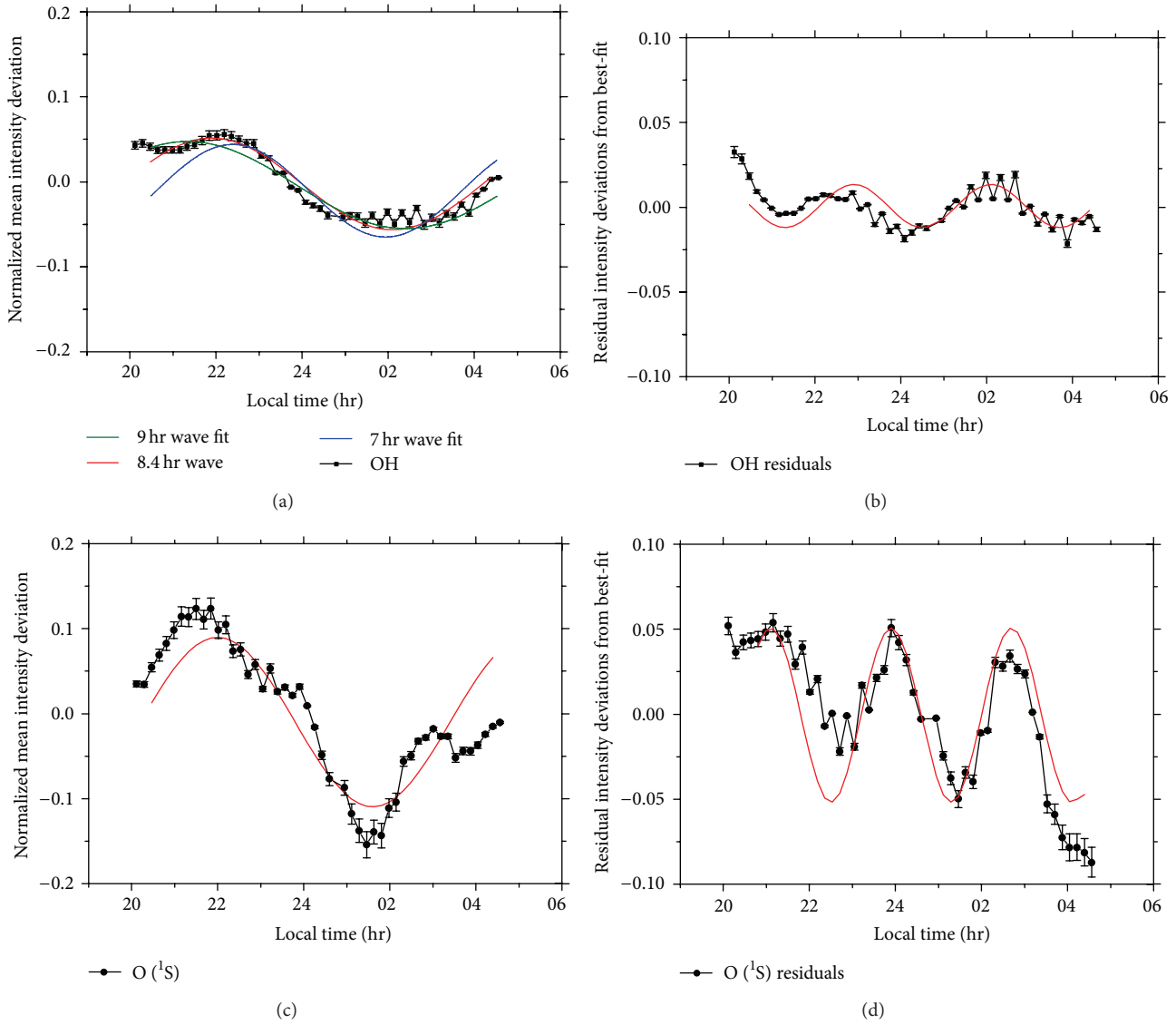

FIGURE 1: The observed nocturnal variability noted on February 9-10, 2010 in OH (a, b) and O (^{1}S) emission (c, d) intensities. The solid lines in each plot exhibit the best-fit model results. (a, c) show the intensity deviations from the nightly average, normalized to their nightly averages. (a) shows the sample wave-fit results for two other wave modes together with the selected 8.4 hr wave. One may note the presence of principal nocturnal wave (a, c) and residual wave (b, d) in the data.

Figure 1(a) together with the chosen one for 8.4 hr. It is evident that other wave-fits do not represent the variability and, therefore, the presence of 8.4 hr wave was finalized. We fitted same wave period obtained from OH data to the O (^{1}S) mean intensity deviations to obtain the amplitude and phase of this wave. Analysis reveals the wave amplitude to be ~6.8%. This indicates that wave amplitudes grew while propagating from OH to the O (^{1}S) layers. Thus the airglow data show observed wave amplitude growth to be ~1.7. Also, we note that the minima of phase of this wave occurred at 26.5 h (i.e., 2.5 h LT) in OH data and at ~25.4 h (i.e., 1.4 h LT) in O (^{1}S), suggesting a phase difference of ~0.9 hr. This means that wave was propagating upward. Assuming a layer separation of 10 km, the observed phase difference results in a vertical phase velocity of ~3 m/s. This, in turn, indicates that the vertical wavelength of 8.4 hr wave is ~90 km. It is important to state here that the observed wave amplitude growth is apparent as these signatures represent integrated effects occurring at airglow layer with thickness of ~5–8 km. Nonetheless, we believe the variability is true.

The bottom panels in the Figure 1 show the residual variability obtained by subtracting the best-fit cosine model data from the mean intensity deviations. The best-fit model results on the residuals (Figure 1(b)) show the period of the residual wave to be 3.1 ± 0.3 hr in OH data with ~1.7% oscillation amplitude and minima of phase at ~25.3 h (i.e., 1.3 h LT). The O (^{1}S) data (Figures 1(c) and 1(d)), on the other hand, show the amplitude of 3.1 hr wave oscillation to be ~4% and minima of phase occurring at ~24.6 h. These values result in a wave amplitude growth of ~2.4 and vertical wavelength of

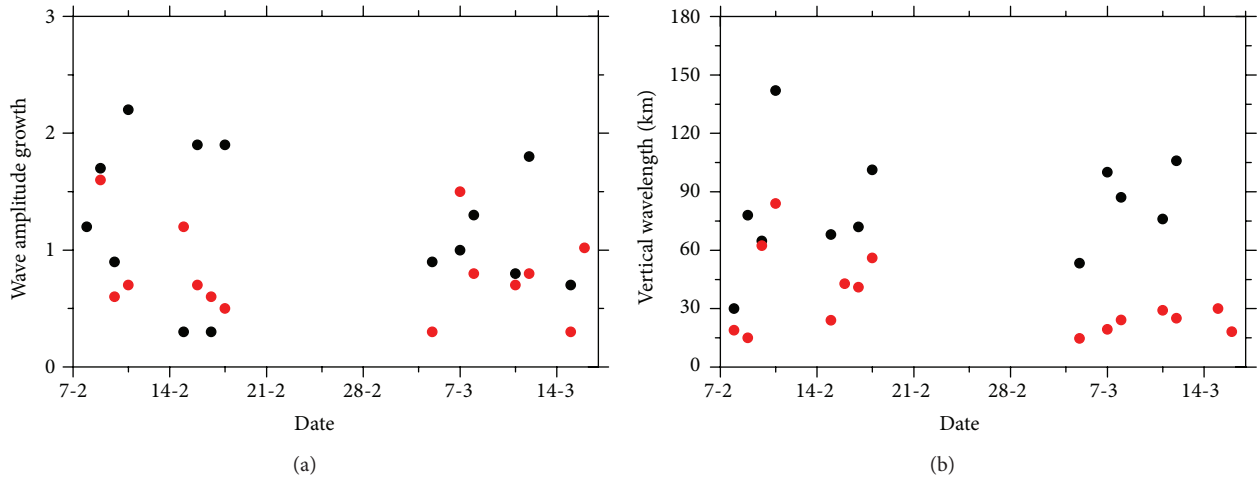

FIGURE 2: Night-to-night variation in the wave amplitude growth (a) and vertical wavelength (b) of the observed waves during February-March 2010 (plotted in month/day format). Filled black and red circles show the results for principal and residual waves, respectively.

~45 km. The plot also suggests that in the presence of several waves the biases may influence the best-fit approximation of wave parameters and one should take due care in the inspection of wave amplitude and phases for the best possible results. Note that the calculation of phase differences is carried out by cross correlating two time series and because most cases show that the identification of minima was better recognized, we have used it for the characterization of vertical wavelengths for the upward propagating waves. Noteworthy in the plot is that residual wave amplitudes are ~1% which may be debated. However, the variability depicting the wave feature is conspicuous with good signal-to-noise ratio. In the wave analysis, we have included only data when wave signatures were evident and their amplitudes were above 0.5%.

We carry out similar best-fit analysis on the nocturnal data of 14 nights of observations to identify the principal as well as residual waves observed during the February and March 2010 campaign. We note that on some nights the primary wave exhibited a very long-period trend whose periodicities could not be identified with the best-fit analysis; therefore, we have not included those long waves. As stated above, the residual waves with oscillation amplitudes below 0.5% were ignored. With the above criteria in place, the results of the best-fit analysis and observed vertical wavelengths are shown in Table 1. Of relevance is that on some days we note the presence of ~11 hr wave in the data which was estimated using best-fitting. Though, we believe that this may be a true representation of variability, the results corresponding to such waves must be further validated using other round-the-clock measurements which at present are not available. These results are summarized in Figure 2. The observed wave characteristics show large variability in terms of wave growth factor and vertical wavelengths. Filled black circles in each plot show the observations corresponding to principal waves while the filled red circles represent the residual waves. We observe that wave growth factor varies from 0.4 to 3.8 for the duration of observation (Figure 2(a)). In general,

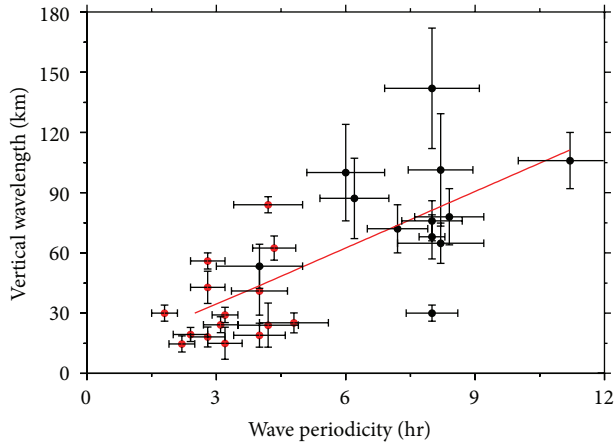

FIGURE 3: Relation between the wave periodicity and their estimated vertical wavelengths. Filled black and red circles show the results for principal and residual waves, respectively.

a wave which is propagating from 87 to 97 km without any dissipation should have a wave amplitude growth ~2 in order to conserve its energy. Therefore, our data clearly indicate that most of the waves observed in our data were dissipated and only few of them were nearly freely propagating. This is somewhat similar to the findings of Taori et al. [16] where wave amplitude growth values were reported to vary from ~0.4 to 4 with most of the waves exhibiting severe dissipation over Maui (20.8°N, 156.2°W).

The vertical wavelengths deduced from the observed phase differences at two emission layers for the observed waves are plotted in Figure 2(b). We note that most of the observed waves have vertical wavelengths varying from 25 km to 75 km. We investigate the possible relation between the wave period and vertical wavelengths in Figure 3. We note that a near linear relation exists between them, with most of the short period waves having smaller vertical wavelengths compared to the longer period ones. The linear best-fit

Table 1: Observed wave characteristics over Kolhapur during the February-March 2010 campaign are shown for each night (first and second rows on each night show principal and residual waves). The best-fitted wave periodicity and wave amplitudes are shown together with the goodness of fit measured as χ^2 values.

Date	Wave period (hr)	Goodness of fit (χ^2)	OH-wave amplitude (%)	O (^{1}S)-wave amplitude (%)	Approximate vertical wavelength (km)	Damping factor
08-Feb-2010	7.8 ± 1.3	0.72	3.5 ± 0.3	3.8 ± 0.5	32 ± 4	0.88
	3.9 ± 0.3	0.78	1.1 ± 0.2	1.2 ± 0.7	20 ± 5	0.89
09-Feb-2010	8.4 ± 0.5	0.81	4.1 ± 0.8	5.2 ± 0.5	76 ± 14	0.68
	3.1 ± 0.3	0.76	1.1 ± 0.7	4.5 ± 0.6	45 ± 6	0.20
10-Feb-2010	8.2 ± 1.3	0.76	17.0 ± 2.1	15.9 ± 4.1	65 ± 10	1.09
	4.3 ± 0.9	0.77	8.1 ± 1.8	10.1 ± 3.8	62 ± 8	0.69
11-Feb-2010	8.0 ± 2.1	0.68	11.1 ± 2.9	15.6 ± 3.5	160 ± 30	0.52
	4.2 ± 0.8	0.83	7.1 ± 2.6	5.9 ± 1	84 ± 6	1.26
15-Feb-2010	7.9 ± 1.3	0.74	18.4 ± 3.1	11.2 ± 1.8	80 ± 11	1.69
	4.2 ± 0.7	0.66	12.0 ± 2.7	10.3 ± 1.3	28 ± 4	1.22
16-Feb-2010	9.2 ± 1.6	0.69	2.0 ± 0.6	2.6 ± 0.4	N/A	0.61
	2.8 ± 0.5	0.85	1.2 ± 0.2	1.3 ± 0.8	40 ± 11	0.90
17-Feb-2010	7.2 ± 1.4	0.89	9.0 ± 1.2	5.6 ± 0.8	72 ± 12	1.67
	4.0 ± 1.1	0.92	4.9 ± 0.4	4.1 ± 0.9	41 ± 8	1.25
18-Feb-2010	8.2 ± 1.3	0.79	17.8 ± 3.1	23.7 ± 5.6	109 ± 28	0.60
	2.8 ± 0.3	0.93	8.6 ± 1.2	6.7 ± 2.8	56 ± 12	1.36
05-Mar-2010	4.0 ± 0.2	0.87	18.0 ± 2.9	17.4 ± 3.7	53 ± 11	1.05
	2.2 ± 0.1	0.88	4.5 ± 0.5	3.2 ± 0.8	14 ± 4	1.47
07-Mar-2010	6.0 ± 1.1	0.75	9.8 ± 0.9	9.8 ± 1.4	100 ± 24	1.00
	2.4 ± 0.2	0.72	1.9 ± 0.2	1.1 ± 0.1	16 ± 4	1.73
08-Mar-2010	6.2 ± 0.9	0.86	7.2 ± 1.1	8.1 ± 1.8	88 ± 20	0.83
	3.1 ± 0.4	0.71	2.0 ± 0.1	2.4 ± 0.3	24 ± 3.5	0.75
11-Mar-2010	8.0 ± 0.7	0.92	16.0 ± 2.8	14.5 ± 1.8	80 ± 10	1.14
	3.2 ± 0.3	0.69	1.7 ± 0.2	1.5 ± 0.1	29 ± 4	1.17
12-Mar-2010	11.2 ± 1.2	0.84	17.7 ± 3.1	22.9 ± 4.6	112 ± 14	0.64
	4.8 ± 0.5	0.77	4.6 ± 0.9	3.9 ± 0.4	27 ± 3.8	1.22
15-Mar-2010	12 ± 1.9	0.93	19.4 ± 2.4	16.8 ± 2.2	N/A	1.20
	1.8 ± 0.2	0.79	4.4 ± 0.4	4.0 ± 0.4	18 ± 5	1.13
16-Mar-2010	2.8 ± 0.2	0.65	6.4 ± 0.8	7.9 ± 1.1	N/A	0.70
	8.4 ± 0.6	0.76	3.5 ± 0.3	2.1 ± 0.2	17 ± 4	1.73

assessment of their relation reveals the dependency to be as follows with r^2 values being 0.54:

$$\text{vertical wavelength} = 6.2 + 9.3 \times \text{wave periodicity}. \quad (2)$$

It is important to state here that highly varying wave saturation and dissipation processes occurring at mesospheric altitudes may lead this relationship to vary. Over equatorial latitudes, Taylor et al. [26] also investigated the relationship between different wave parameters. They used image data to characterize very short period waves and with the help of coincident lidar data they showed that vertical wavelength and wave periodicity (5 to 20 min periods) have a relation. They reported large vertical wavelengths for shorter period waves which differ from our observations (though wave periods >20 min based on the lidar data showed a different dependency which agrees well with our result). In a recent investigation Taylor et al. [9] investigated relations between horizontal wavelength and wave periods in a 5 min to 90 min range and found a positive correlation which was explained by a power law. The gravity wave dispersion relation suggests that $\iota/T = \lambda z/\lambda x$, where ι is natural oscillation period, T is wave period, λz is vertical wavelength, and λx is horizontal wavelength. It is therefore implied that if ι and T are fixed then, as λz increases, λx shall increase. Based on the above argument, our results are in agreement with that of Taylor et al. [9] which suggests a positive correlation between wave period and horizontal wavelengths.

3.2. Wind Variation and Observed Vertical Propagation of Wave. The vertical wave propagation and variation of wave

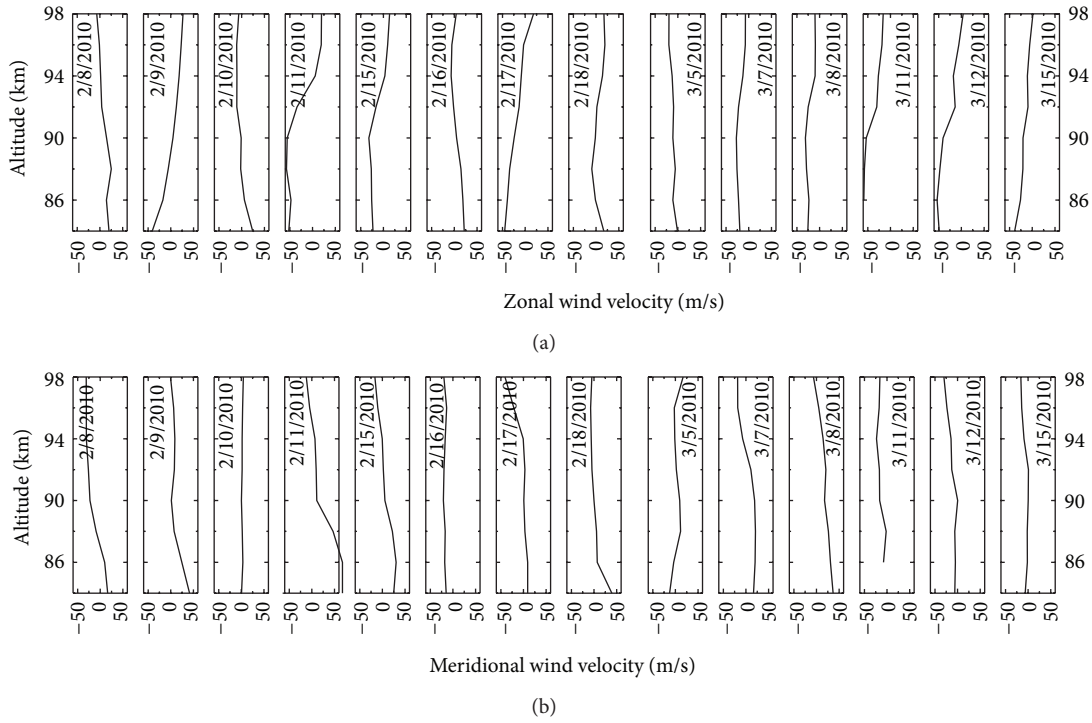

Figure 4: Observed mean zonal (a) and meridional (b) wind variability corresponding to the night airglow observations during February and March.

amplitudes depends on the dissipation/filtering processes. The observed wave periods in our data suggest that these waves were not completely dissipated while propagating from OH layer to the O (^{1}S) layer. The interaction of waves with the mean wind is the most important dissipation mechanism (e.g., [2]). It is known that upward propagation of waves depends on the horizontal propagation direction of waves and zonal wind characteristics. The direction of wave propagation may vary from one season to another (eg., [27]). It would be ideal to have the gravity wave propagation directions through image data for suitable wind and wave interaction study. However, we investigate this with the help of coincident zonal and meridional winds (e.g., [12, 17, 28]).

To scrutinize the effects of winds on wave propagation, in Figure 4, we plot the observed nightly mean zonal (Figure 4(a)) and meridional (Figure 4(b)) wind variation (time averaged from 1800 h LT to 2800 h LT, i.e., averaging from evening to early morning) corresponding to the night airglow observations. We observe large variation from one night to another. The nightly mean zonal winds, in particular at ~86 km altitude in February 2010, show oscillating nature; that is, on February 8 zonal winds are eastward, while on February 9 they turn westward which continues till the end of February 2010. In March 2010, however, at ~86 km, winds are mostly westward. The meridional winds also reveal the oscillatory nature from one night to the other; however, at about 94 km most of the time they are southward. The temporal variation of the winds shows a strong semidiurnal tide to be present in the data which show a gradual variation. To elaborate this, we plot the zonal wind variability in Figure 5 for February 9-10, 2010. It is evident with best-fit (red curve) that a semidiurnal tidal feature was dominant in wind data. For a comparison with OH data, we carry out a Fourier analysis of residual (from best-fit) wind variability and OH intensity data. Figure 5 shows the results of the Fourier analysis. It is clear that the spectrum at both data indicates that the wave periods are somewhat similar. This emphasis that the cause of wind variability as well as the OH intensity variability are wave processes of similar nature. This is an interesting aspect which needs to be further investigated. However, the aim of the present investigation is to find out a link between wave parameters and wind shears; at present, we limit our discussion on this aspect. Because of the nocturnal variability noted in the wind data, we believe that it should be the vertical shears that would affect the vertical propagation characteristics. Therefore, we computed the wind shears at 87–97 km altitudes. We observe that on February 8, 9, and 16 the wind shear magnitudes are smaller than that observed on other nights. The relation between the wind shears and wave dissipation is discussed in the following section.

3.3. Wave Damping. The amplitude growth of the waves observed at OH and O (^{1}S) emission altitudes can be translated into a damping factor. Numerical investigations by Liu and Swenson [17] and Vargas et al. [18] estimated the damping rates of upward propagating waves at O_2, OH, and O (^{1}S) emission layers. Using the observations discussed in Section 3.1, we calculate the damping factors as explained in (1). The estimated damping factors are plotted in Figure 6 against the observed vertical wavelengths. We find that

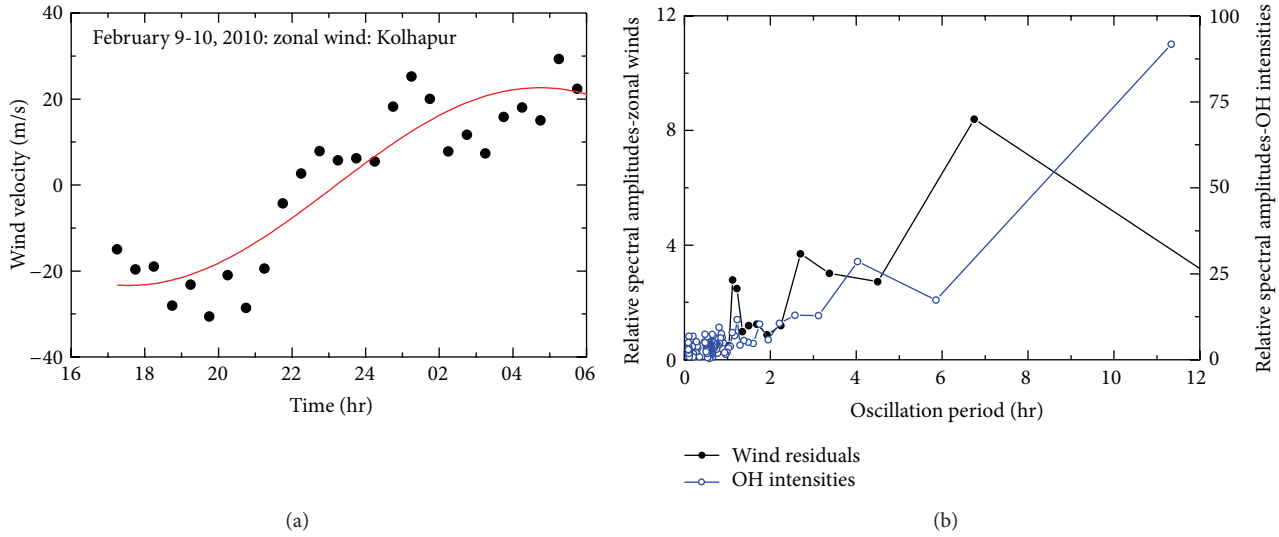

Figure 5: The averaged zonal wind variability during 1800 h to 0600 h on February 9-10, 2010 for 86–92 km altitudes (a). The Fourier analysis of zonal residual winds and OH intensity data shown in the bottom (b) indicate commonality in the period of oscillation in both data.

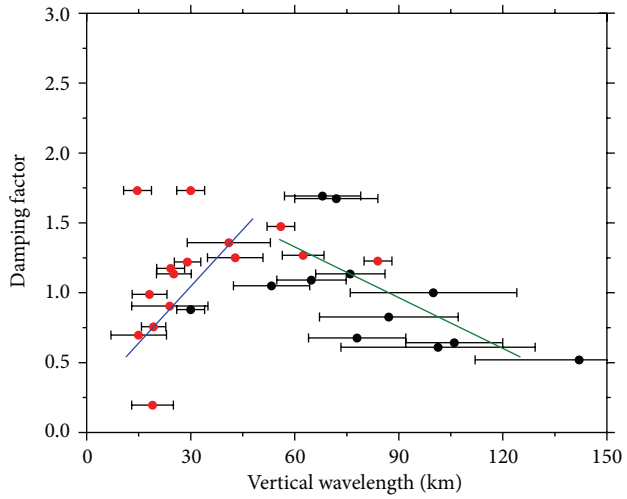

Figure 6: Variation of observed wave damping factors against the observed vertical wavelengths exhibiting a complex relation.

the damping factors for the observed waves change from 0.2 to 1.9. This suggests that no wave freely propagated during the observation period under consideration which is in agreement with earlier reports (e.g., [19, 29]). Interestingly, on occasion, few waves with vertical wavelengths 20–50 km were propagating upwards without having significant damping (in fact, they show large variation, β values from 0.2 to 1.7), while more than 50% waves were either saturated or damped. We note that at shorter than 40 km vertical wavelengths, the damping factors increase with increasing vertical wavelengths. On the other hand, the vertical wavelengths show a negative correlation with the damping factors. In this regard, Takahashi et al. [19] investigated a relation between vertical wavelength and damping factors. They found wave amplitude growth to have a positive relation with vertical wavelengths and that the damping factors decrease with increasing vertical wavelengths which is similar to our results. Important to note is that numerical study of Vargas et al. [18] shows that for vertical wavelengths varying from ~15 km to 50 km, wave amplitude growth decreases from 1.8 to 1.4, which possibly explains the reason for large scatter for shorter than 30 km vertical wavelengths in Figure 6. Also, they suggest that the wave amplitude growth varies from 0.6 to 2.0 for vertical wavelengths varying from 15 to 50 km, which broadly agrees with our results.

Further, as explained earlier, wind shears may be a responsible factor for observed wave amplitude growth and hence the damping factor; we plot the damping factors against the observed wind shears between 87 and 97 km altitudes in Figure 7. In the absence of direction of wave propagation, we investigate the effects of zonal as well as meridional wind shears on the estimated wave damping factors. We note that with increasing zonal wind shears (Figure 7(a)), damping factors tend to increase. The linear best-fit analysis shows the following relation ($r^2 = 0.18$) between damping factor and zonal wind shears. In our analysis we have taken the difference in the wind velocity between 87 km and 97 km as a measure of wind shears:

$$\text{damping factor} = 0.75 + 0.007 \times \text{zonal wind shear}. \quad (3)$$

The poor r^2 obviously suggests that most probably gravity wave propagation vector is not inclined to the zonal plane and may have a strong meridional propagation. To investigate this we carry out same analysis on the meridional winds. We note that the damping factors show somewhat better relation with the meridional wind shears. The linear fit shows the r^2 value to be 0.49 with the following relation:

$$\text{damping factor} = 1.26 + 0.016 \times \text{meridional wind shear}. \quad (4)$$

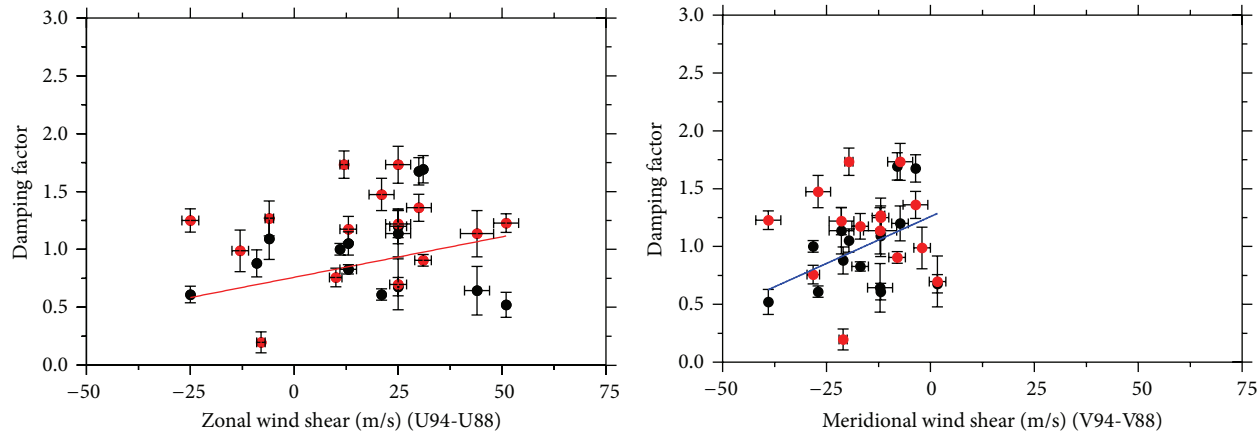

FIGURE 7: The distribution of damping factors with respect to the observed zonal (a) and meridional (b) wind shears between 87 and 94 km altitudes. Filled black and red circles show the results for principal and residual waves, respectively.

Further, the damping factors of principal waves (filled black circles) show better dependency on the wind shears, while the shorter period (residual wave) ones show a large scatter which may be affecting the deduced r^2 values. It is interesting to note that most of the time meridional winds were southward and as the wind shears tend to become northward damping factor increases. Similarly, in zonal direction, as the wind shears tend to be more eastward, damping increases. This in turn suggests that possibly observed waves had a stronger meridional component compared to the zonal component and have preferential north-eastward movement. Though, simultaneous image measurements are not available at present, earlier results from Indian sector have shown that most of the time the gravity waves show strong northward propagation (e.g., [20, 30, 31]) which supports our assertion. Though it is understood that horizontal and vertical propagation characteristics depend on the wind filtering, we show that not only the propagation but also the observed amplitude growth/damping factor of the waves depends on the wind shears which have an important bearing on the heat and momentum transfer. However, our results are based on a limited data; these conclusions are tentative and must be confirmed by further study.

4. Conclusions

Our night airglow measurements from the low latitude Indian station, Kolhapur, (16.8°N, 74.2°E) during February and March 2010 lead to the following conclusions.

(1) Mesospheric airglow data show large variability in the gravity wave amplitudes.

(2) Most of the upward propagating waves observed in both the OH and O (^{1}S) emission altitudes show amplitude growth varying from 0.4 to 3.8.

(3) The data reveal a positive correlation between wave periodicity and vertical wavelength.

(4) The waves having vertical wavelengths less than 40 km show a positive correlation with damping factors, while the larger ones show negative correlation.

(5) The damping factors of waves show a positive correlation with the zonal and meridional wind shears.

In conclusion, because the present investigation is based on limited data, a wider study is required to confirm the conclusions drawn here. Further, the effects of these wave processes on the thermosphere-ionosphere system need to be established with coordinated measurements in the near future.

Conflict of Interests

The authors declare that there is no conflict of interests regarding the publication of this paper.

Acknowledgments

This work is a collaborative work under CAWSES-India Phase II, theme-3 and SAFAR between National Atmospheric Research Laboratory, Gadanki, India, and Indian Institute of Geomagnetism, Mumbai, India. The data used in the present investigation belongs to India and Indian Institute of Geomagnetism, Mumbai, India, and can be obtained by sending a data request to rupeshghodpage@gmail.com with a copy of request to gurubra@iigs.iigm.res.in.

References

[1] W. K. Hocking, "Dynamical coupling processes between the middle atmosphere and lower ionosphere," *Journal of Atmospheric and Terrestrial Physics*, vol. 58, no. 6, pp. 735–752, 1996.

[2] D. C. Fritts and M. J. Alexander, "Gravity wave dynamics and effects in the middle atmosphere," *Reviews of Geophysics*, vol. 41, no. 1, 2003.

[3] M. C. Kelley, M. F. Larsen, C. LaHoz, and J. P. McClure, "Gravity wave initiation of equatorial spread F: a case study," *Journal of*

Geophysical Research: Space Physics, vol. 86, no. 11, pp. 9087–9100, 1981.

[4] I. Paulino, H. Takahashi, A. F. Medeiros et al., "Mesospheric gravity waves and ionospheric plasma bubbles observed during the COPEX campaign," *Journal of Atmospheric and Solar-Terrestrial Physics*, vol. 73, no. 11-12, pp. 1575–1580, 2011.

[5] H. Takahashi, M. J. Taylor, P. D. Pautet et al., "Simultaneous observation of ionospheric plasma bubbles and mesospheric gravity waves during the SpreadFEx campaign," *Annales Geophysicae*, vol. 27, no. 4, pp. 1477–1487, 2009.

[6] A. Taori, J. J. Makela, and M. Taylor, "Mesospheric wave signatures and equatorial plasma bubbles: a case study," *Journal of Geophysical Research A: Space Physics*, vol. 115, no. 6, 2010.

[7] A. Taori, A. K. Patra, and L. M. Joshi, "Gravity wave seeding of equatorial plasma bubbles: An investigation with simultaneous F region, e region, and middle atmospheric measurements," *Journal of Geophysical Research A*, vol. 116, no. 5, 2011.

[8] A. Taori, N. Dashora, K. Raghunath, J. M. Russell III, and M. G. Mlynczak, "Simultaneous mesosphere-thermosphere-ionosphere parameter measurements over Gadanki (13.5◦N, 79.2◦E): first results," *Journal of Geophysical Research: Space Physics*, vol. 116, no. 7, Article ID A07308, 2011.

[9] M. J. Taylor, P.-D. Pautet, A. F. Medeiros et al., "Characteristics of mesospheric gravity waves near the magnetic equator, Brazil, during the SpreadFEx campaign," *Annales Geophysicae*, vol. 27, no. 2, pp. 461–472, 2009.

[10] S. M. I. Azeem and G. G. Sivjee, "Multiyear observations of tidal oscillations in OH M(3,l) rotational temperatures at South Pole, Antarctica," *Journal of Geophysical Research*, vol. 114, no. 6, Article ID A06312, 2009.

[11] P. R. Fagundes, H. Takahashi, Y. Sahai, and D. Gobbi, "Observations of gravity waves from multispectral mesospheric nightglow emissions observed at 23°S," *Journal of Atmospheric and Solar-Terrestrial Physics*, vol. 57, no. 4, pp. 39–40, 1995.

[12] A. F. Medeiros, R. A. Buriti, E. A. Machado et al., "Comparison of gravity wave activity observed by airglow imaging at two different latitudes in Brazil," *Journal of Atmospheric and Solar-Terrestrial Physics*, vol. 66, pp. 647–654, 2004.

[13] J. F. Noxon, "Effects of internal gravity waves upon night airglow temperatures," *Geophysical Research Letters*, vol. 5, no. 1, pp. 25–27, 1978.

[14] E. R. Reisin and J. Scheer, "Characteristics of atmospheric waves in the tidal period range derived from zenith observations of O_2(0-1) atmospheric and OH(6-2) airglow at lower midlatitudes," *Journal of Geophysical Research D*, vol. 101, no. 16, pp. 21223–21232, 1996.

[15] A. Taori, M. J. Taylor, and S. Franke, "Terdiurnal wave signatures in the upper mesospheric temperature and their association with the wind fields at low latitudes (20◦N)," *Journal of Geophysical Research*, vol. 110, no. 9, pp. 1–12, 2005.

[16] A. Taori, A. Guharay, and M. J. Taylor, "On the use of simultaneous measurements of OH and O_2 emissions to investigate wave growth and dissipation," *Annales Geophysicae*, vol. 25, no. 3, pp. 639–643, 2007.

[17] A. Z. Liu and G. R. Swenson, "A modeling study of O_2 and OH airglow perturbations induced by atmospheric gravity waves," *Journal of Geophysical Research*, vol. 108, no. 4, p. 4151, 2003.

[18] F. Vargas, G. Swenson, A. Liu, and D. Gobbi, "O(^{1}S), OH, and O_2 (b) airglow layer perturbations due to AGWs and their implied effects on the atmosphere," *Journal of Geophysical Research*, vol. 112, Article ID D14102, 2007.

[19] H. Takahashi, A. Onohara, K. Shiokawa, F. Vargas, and D. Gobbi, "Atmospheric wave induced O_2 and OH airglow intensity variations: effect of vertical wavelength and damping," *Annales Geophysicae*, vol. 29, no. 4, pp. 631–637, 2011.

[20] G. K. Mukherjee, "The signature of short-period gravity waves imaged in the OI 557.7 nm and near infrared OH nightglow emissions over Panhala," *Journal of Atmospheric and Solar-Terrestrial Physics*, vol. 65, no. 14-15, pp. 1329–1335, 2003.

[21] A. Taori and N. Parihar, "Simultaneous bi-station measurements of mesospheric waves from Indian low latitudes," *Advances in Space Research*, vol. 48, no. 2, pp. 218–226, 2011.

[22] N. Parihar, S. Gurubaran, and G. K. Mukherjee, "Observations of OI 557.7 nm nightglow at Kolhapur (17◦ N), India," *Annales Geophysicae*, vol. 29, no. 10, pp. 1873–1884, 2011.

[23] A. Taori and M. Taylor, "Characteristics of wave induced oscillations in mesospheric O_2 emission intensity and temperatures," *Geophysical Research Letters*, vol. 33, Article ID L01813, 2006.

[24] R. Rajaram and S. Gurubaran, "Seasonal variabilities of low-latitude mesospheric winds," *Annales Geophysicae*, vol. 16, no. 2, pp. 197–204, 1998.

[25] J. Yee, G. Crowley, R. G. Roble, W. R. Skinner, M. D. Burrage, and P. B. Hays, "Global simulations and observations of O(^{1}S), $O_2(^1\sum)$ and OH mesospheric nightglow emissions," *Journal of Geophysical Research A: Space Physics*, vol. 102, no. 9, pp. 19949–19968, 1997.

[26] M. J. Taylor, W. R. Pendleton Jr., S. Clark, H. Takahashi, D. Gobbi, and R. A. Goldberg, "Image measurements of short-period gravity waves at equatorial latitudes," *Journal of Geophysical Research D: Atmospheres*, vol. 102, no. 22, pp. 26283–26299, 1997.

[27] A. F. Medeiros, H. Takahashi, R. A. Buriti, K. M. Pinheiro, and D. Gobbi, "Atmospheric gravity wave propagation direction observed by airglow imaging in the South American sector," *Journal of Atmospheric and Solar-Terrestrial Physics*, vol. 67, no. 17-18, pp. 1767–1773, 2005.

[28] R. S. Lindzen, "Turbulence and stress due to gravity wave and tidal breakdown," *Journal of Geophysical Research*, vol. 86, pp. 9707–9714, 1981.

[29] A. Taori and V. Kamalakar, "Airglow measurements of wave damping at upper mesospheric altitudes over a low latitude station in India," *Indian Journal of Radio & Space Physics*, vol. 42, no. 5, pp. 371–379, 2013.

[30] V. Lakshmi Narayanan, S. Gurubaran, and K. Emperumal, "Imaging observations of upper mesospheric nightglow emissions from Tirunelveli (8.7◦N)," *Indian Journal of Radio and Space Physics*, vol. 38, no. 3, pp. 150–158, 2009.

[31] A. Taori, A. Jayaraman, and V. Kamalakar, "Imaging of mesosphere-thermosphere airglow emissions over Gadanki (13.5◦N, 79.2◦E)—first results," *Journal of Atmospheric and Solar-Terrestrial Physics*, vol. 93, pp. 21–28, 2013.